ACS SENSORS

pubs.acs.org/acssensors

Article

Wireframe Orbit-Accelerated Bipedal DNA Walker for Electrochemiluminescence Detection of Methyltransferase Activity

Mei-Chen Pan, Mao-Hua Gao, Xia Yang, Wen-Bin Liang, Ruo Yuan, and Ying Zhuo*

Cite This: *ACS Sens.* 2022, 7, 2475−2482

Read Online

ACCESS | Metrics & More | Article Recommendations | Supporting Information

ABSTRACT: In spite of the DNA walkers executing the signal accumulation task in the process of moving along the predetermined paths, the enhancement of walking dynamics and walking path controllability are still challenging due to the unprogrammed arrangements of DNA orbits. Taking these dilemmas into account, a bipedal DNA walker was designed skillfully by the virtue of wireframe orbits assembled by DNA cubes in order, which improved the efficiency and the continuity of walking. It could be attributed to the fact that both the contact chance and the dynamic interaction between walking strands and designated orbits were beneficial to minimize the possibility of derailment and improve the accumulation of signal. In addition, the hollow titanium dioxide nanospheres coated with rubrene (Rub@TiO_2 NSs) were prepared by the etching of inner silicon dioxide nanoparticles (SiO_2 NPs) to regulate the distribution pattern of rubrene (Rub) molecules and expose more electrochemically active sites for high-efficient electrochemiluminescence (ECL). Benefiting by the pore confinement-enhanced ECL, the electron and mass transfer was significantly accelerated because of the hollow structure of Rub@TiO_2 NSs. Subsequently, endogenous dissolved oxygen as the coreactant and palladium nanoparticles (Pd NPs) as the coreaction accelerator were employed to constitute a ternary ECL system with explosive signal response. Combining with this ECL platform, the bipedal walker activated by the target can autonomously and directionally move on the DNA wireframe orbits to release the quenching probes continuously. In this way, the biosensor displayed a low detection limit (2.30×10^{-8} U·mL^{-1}) and a wide linear range (1.0×10^{-7} to 1.0×10^{-1} U·mL^{-1}) for the sensitive detection of Dam methyltransferase (Dam MTase) activity. Therefore, a novel strategy for the accurate quantification of epigenetic targets was developed by virtue of improving the walking dynamics of DNA walker and amplifying the ECL of Rub molecules.

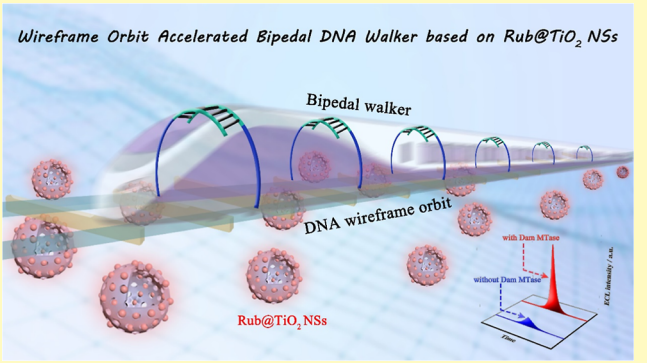

KEYWORDS: *electrochemiluminescence biosensor, wireframe orbit, bipedal DNA walker, hollow TiO_2 nanospheres coated with rubrene, Dam methyltransferase*

INTRODUCTION

DNA walker, as an exceptional nucleic acid amplification, could execute the signal accumulation task in the process of autonomous and stepwise movement on the predetermined orbits, by virtue of the programmable target-specific sequences and computational controlled power.[1] However, conventional DNA walkers relying on random assembly were inadequate in walking kinetics and continuity because the disordered arrangement of orbits increased the risks of walking derailment and interruption.[2] Hence, well-ordered and continuous orbits are still highly desirable, although challenging.[3,4] Given the considerations, DNA framework structures that could be tailored artificially with endless possibilities, may be capable of meeting these challenges in the improvement of walking kinetics and continuity.[5] Recently, Yang and co-operators designed a DNAzyme walker using a quadrilateral nucleic acid frame to colocalize the walkers and orbits for the readout signal amplification.[6] Although the kinetic of the reaction was improved, the problems of walking controllability and continuity still remained due to the lack of connections between each unit. Compared with DNA double strands or DNA tetrahedrons, the wireframes assembled by DNA cubes possessed desirable rigid frameworks and extended possibility, which provided the assistance for the fabrication of ordered and controllable orbits.[7] Moreover, the continuous orbits could control the walking direction and greatly reduce the likelihood of derailment.[8] Inspired by this, ordered and extended wireframe orbits were constructed elaborately by the assembly of DNA cubes for the autonomous and directional walking in

Received: June 15, 2022
Accepted: August 8, 2022
Published: August 17, 2022

https://doi.org/10.1021/acssensors.2c01262
ACS Sens. 2022, 7, 2475−2482

this work, which could substantially contribute to the improvement of walking efficiency and continuity of the DNA walker.

Organic optoelectronic species, including dyes molecules and conducting polymers, have many merits of controllable initial intramolecular charge transfer, high thermal stability and photostability in the electrochemiluminescence (ECL) field.[9] Mostly, the organic ECL dyes with large π-conjugated aromatic structures, such as rubrene (Rub), were recently applied as ECL emitters, and the emissive mechanisms were revealed based on the theory of through-bond conjugation.[10] According to the argument of Najafov et al., the photoconductivity in Rub crystals mostly originated from surface effects because of singlet fission, followed by triplet exciton diffusion to the surface where they dissociated.[11] By the inspiration of pore confinement-enhanced ECL, the matrixes with hollow carrier structures have great potential in accelerating the electron and mass transfer to enhance the ECL efficiency of rubrene in comparison to common Rub microblocks synthesized by the reprecipitation method.[12] Meanwhile, the hollow matrix could make emitters feasible for self-assembly to expose more active sites, as well as maximize the reactive free radical cavity. Interestingly, titanium dioxide (TiO_2) has been considered as a promising and efficient photoelectric material by virtue of high photoelectric conversion efficiency, good biocompatibility, and effective binding ability with Rub.[13] Thus, hollow TiO_2 nanomaterial was an ideal matrix, which may supply a useful microenvironment to tune the distribution pattern of Rub and reinforce charge transport.[14] Herein, the hollow TiO_2 nanospheres coated with rubrene (Rub@TiO_2 NSs) were prepared with the inner nanoparticles (SiO_2 NPs) as sacrifice cores to expose more active sites, demonstrating outstanding ECL intensity and stability of Rub, which has not been reported so far.

DNA methyltransferases (MTase), catalyzing the transfer of the methyl groups from *S*-adenosyl-L-methionine (SAM) molecules to the adenine/cytosine (A/C) residues in the specific genomic DNA, are considered as potential candidates for diagnosing the diseases related to epigenetics.[15,16] Generally, the efficient recognition and signal amplification were two important elements in the construction of biosensors for the detection of MTase activity. Herein, the bipedal walker activated by target MTase (Dam MTase) with the catalysis role in DNA modification was designed, which autonomously and directionally moved on the ordered DNA framework orbits to release the quenching probes continuously. Ultimately, the sensitive analysis of Dam MTase activity was achieved by the detection of ECL signal recovery relying on the ternary ECL system with Rub@TiO_2 NSs as the ECL emitter, endogenous dissolved oxygen as the coreactant, and palladium nanoparticles (Pd NPs) as coreaction accelerators.[12,17] Therefore, this work provided new paradigms by combining the improvement strategies of DNA walker and ECL performance for sensitive and noninvasive detection of enzymatic activity.

EXPERIMENTAL SECTION

Synthesis of the Rub@TiO_2 NSs. First, the SiO_2 NPs were synthesized by the typical Stöber method.[18] 3 mL of 25% ammonia solution was dropwise added into 20 mL of ethanol under stirring, following by adding 600 μL tetraethyl orthosilicate rapidly. The mixture was stirred continuously for 4 h, and the SiO_2 NPs were separated by centrifugation, washed three times with ethanol and water successively, and then dried under vacuum at 80 °C for 6 h.

Whereafter, the TiO_2@SiO_2 NPs were prepared through a sol−gel method.[19] To be specific, 5 mg of SiO_2 NPs was dispersed adequately in 50 mL of ethanol, and then, 0.3 mL of deionized water, 0.15 g of hydroxypropyl cellulose, and 0.85 mL of tetrabutylorthotitanate were added into the mixed solution in sequence. After stirring for 15 min, the resultant solution was held for 3 h. TiO_2@SiO_2 NPs were collected by centrifugation, rinsed three times with ethanol and deionized water, and dried at 80 °C for 6 h.

Next, 12 mg of the prepared TiO_2@SiO_2 NPs was dispersed in 2 mL of ethanol, and then, 8 mg of Rub powder was added into the mixed ethanol solution for the modification of Rub by the surface oxygen defect of TiO_2.[9] After stirring to react for 4 h, the Rub@TiO_2@SiO_2 NPs were centrifuged and rinsed with deionized water three times. To etch the inner SiO_2 NPs, the resultant Rub@TiO_2@SiO_2 NPs were dispersed in 5 mL of 1.2 M NaOH aqueous solution to stir at 60 °C for 4 h.[20] As a result, the product was isolated by centrifugation and washed with deionized water and then dispersed in 5 mL of deionized water for further use.

Process of Sample Preparation and the Activation of Bipedal DNA Walker. Two hairpin DNA strands (H1, H2) were dissolved in Tris−EDTA buffer and annealed from 95 to 25 °C in 3 h, respectively, and then, these two hairpin strands were mixed and reacted at 37 °C for 2 h to prepare the unactivated bipedal DNA walkers with double-hairpin structure (DH). Then, 10 μL 5 μM DH solution, 5 μL 160 μM SAM, 5 μL 10× Dam MTase buffer, 28 μL RNase-free water, and 2 μL Dam MTase with different concentrations were mixed to a total volume of 50 μL and reacted at 37 °C for 2 h to methylate the A residue in the palindromic sequence of 5′-G-A-T-C-3′. Following that, 2 μL Dpn1 (20 000 U·mL^{-1}), 6 μL 10× CutSmart buffer, and 4 μL RNase-free water were injected into the resultant solution and further reacted at 37 °C for 1 h to prepare the bipedal DNA walker under the cleavage reaction of Dpn1. Next, the mixed sample solution containing bipedal DNA walker was heated at 60 °C for 20 min to stop the cleavage reaction.

Assembly of Wireframe Orbits to Fabricate the ECL Biosensor Platform. The cleaned mirror-like electrode surface of glassy carbon electrode (GCE, Φ = 4 mm) was obtained by referring to the reported literature.[21] 10 μL 15-fold diluted Rub@TiO_2 NSs solution and 8 μL Pd NP solution (the preparation is shown in Supporting Information 1.3) were dropped onto the GCE interface successively and dried at 37 °C to obtain Pd NPs/Rub@TiO_2 NSs/GCE.

Synchronously, each DNA single strand (C_{1-1} ~ C_{1-7}, C_{2-1} ~ C_{2-4}) was diluted by Tris-Mg^{2+} buffer to the final concentration of 4 μM. As regards to the single strands containing thiol groups, C_{1-5} and C_{1-6} were pretreated with 1 M tris-(2-carboxethyl)-phosphine hydrochloride (TCEP) at 37 °C for 1 h to reduce disulfide bonds. Subsequently, DNA single strands (C_{1-1} ~ C_{1-7}) were mixed at equal concentrations and reacted by heating to 95 °C for 10 min and cooling to 4 °C rapidly in order to produce the 0.5 μM DNA cube 1 solution. The 0.5 μM DNA cube 2 solution was prepared with C_{2-1} ~ C_{2-7} by the similar procedure as DNA cube 1. Then, the resultant DNA cube 1 and the DNA cube 2 solution were further mixed evenly and reacted at 37 °C for 2 h to assemble the DNA wireframe orbits. A 10 μL solution containing DNA wireframe orbits was added on the Pd NPs/Rub@TiO_2 NSs/GCE and incubated at 37 °C for another 2 h to acquire the DNA wireframe orbit-modified GCE (DNA wireframe orbits/Pd NPs/Rub@TiO_2 NSs/GCE). Followed by rinsing with phosphatic buffer saline (PBS) solution, 10 μL 1 μM hexanethiol (HT) solution was dripped on the modified GCE at room temperature for 40 min to block nonspecific sites and acquire the ECL biosensing platform.

Measurement Procedure. Dam MTase with different concentrations were used to prepare the standard samples containing the bipedal DNA walker solution by the similar procedure of *Process of Sample Preparation and the Activation of Bipedal DNA Walker*. Subsequently, 10 μL of the sample solution containing bipedal DNA walker converted from Dam MTase was mixed with 2 μL Nt.BbvC1

https://doi.org/10.1021/acssensors.2c01262
ACS Sens. 2022, 7, 2475−2482

Scheme 1. Schematics of the Proposed ECL Biosensor: Synthesis Steps of Hollow Rub@TiO_2 NSs (A); construction Process of ECL Biosensor for Dam MTase Activity Detection Based on the Wireframe Orbit-Accelerated Bipedal DNA Walker (B)

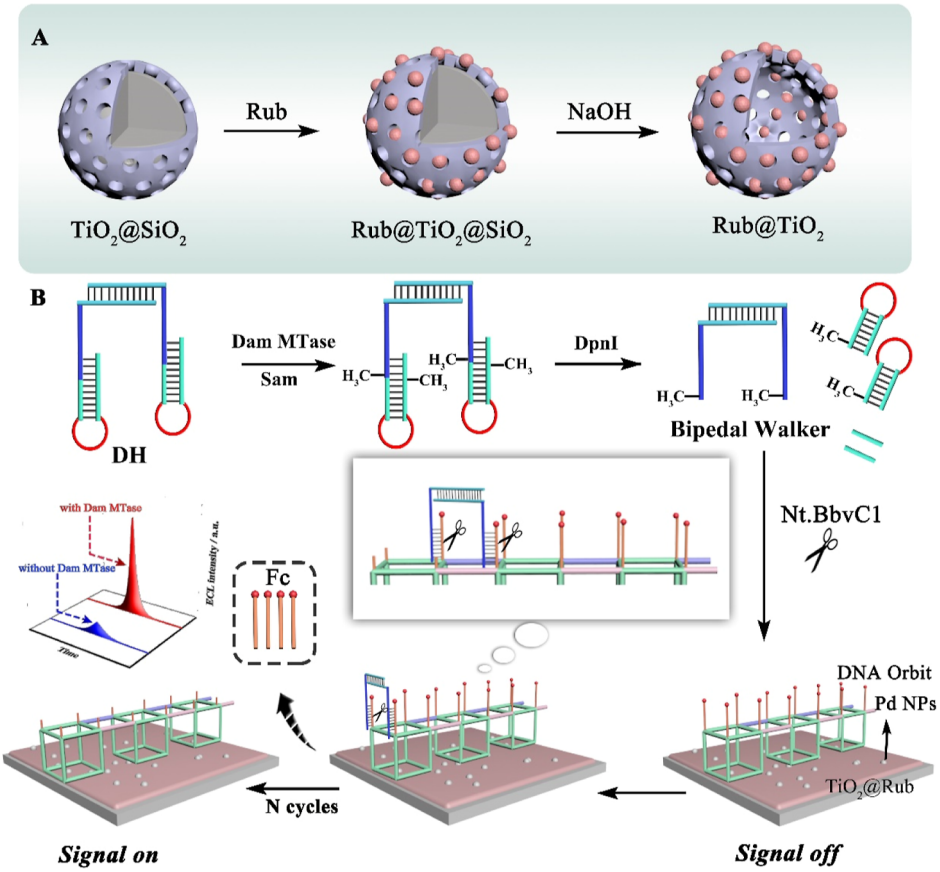

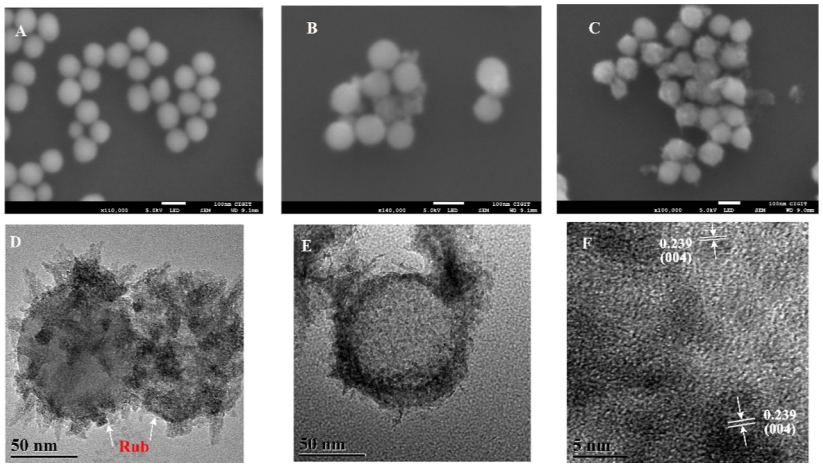

Figure 1. (A) SEM characterizations of the SiO_2 NPs, (B) TiO_2@SiO_2 NPs, and (C) Rub@TiO_2@SiO_2 NPs, at the scale bar of 100 nm, (D) TEM characterizations of the Rub@TiO_2@SiO_2 NPs and (E,F) Rub@TiO_2 NSs. Scale bars are 50 nm in D, E and 5 nm in F.

(2000 U·mL^{-1}), 2 μL 10× CutSmart buffer, and 16 μL RNase-free water, and then, the mixed solution was dropped on the prepared biosensor interface and incubated at 37 °C for 2 h to operate the bipedal walker. After rinsing with PBS, the final biosensor was measured in 2 mL of 0.1 M PBS for ECL signals with an MPI-E ECL system by setting the potential from −1.0 to 1.2 V at a scan rate of 300 mV/s (photomultiplier high-voltage 800 V, magnitude 4).

RESULTS AND DISCUSSION

Design Principle of the ECL Biosensor for Dam MTase Activity Detection. The specific design principle of the ECL biosensor for Dam MTase activity analysis is outlined in Scheme 1. As exhibited in Scheme 1A, taking advantage of the surface oxygen defects of TiO_2, the Rub was deposited on the surface of TiO_2@SiO_2 NPs synthesized in advance by the sol−gel method, and then, the inner SiO_2 NPs as sacrifice cores were etched by the NaOH solution. Subsequently, the ternary ECL system with explosive signal response was prepared with Rub@TiO_2 NSs as the ECL emitters, endogenous dissolved oxygen as the coreactant, and Pd NPs as the coreaction accelerator. Scheme 1B displays the construction process of

https://doi.org/10.1021/acssensors.2c01262
ACS Sens. 2022, 7, 2475−2482

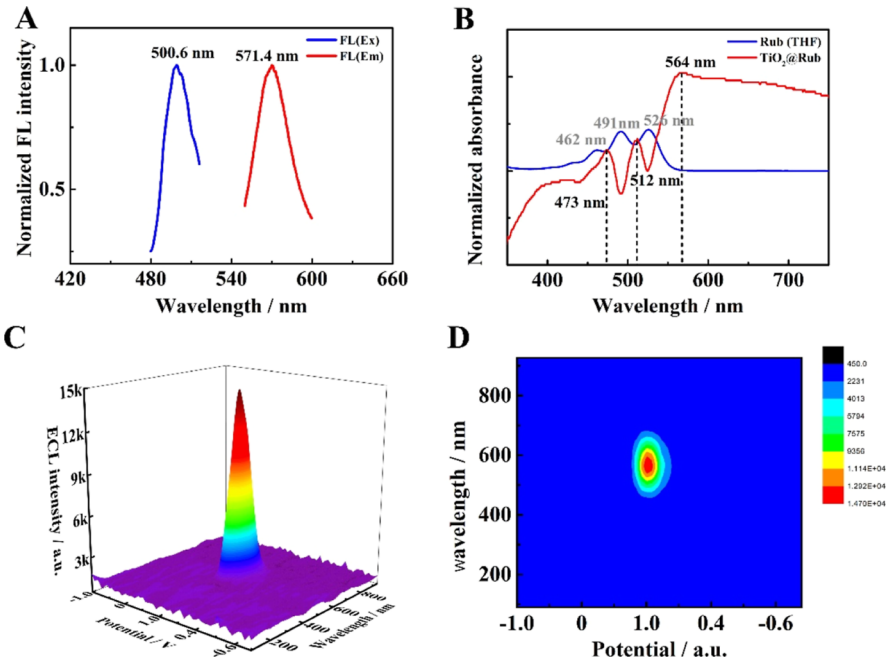

Figure 2. (A) Fluorescence excitation spectrum and emission spectrum of Rub@TiO_2 NSs. (B) Uv−visible absorption spectra of Rub (THF) and Rub@TiO_2 NSs. (C) ECL spectrum of the Rub@TiO_2 NSs; (D) 3D ECL color map surface of the Rub@TiO_2 NSs.

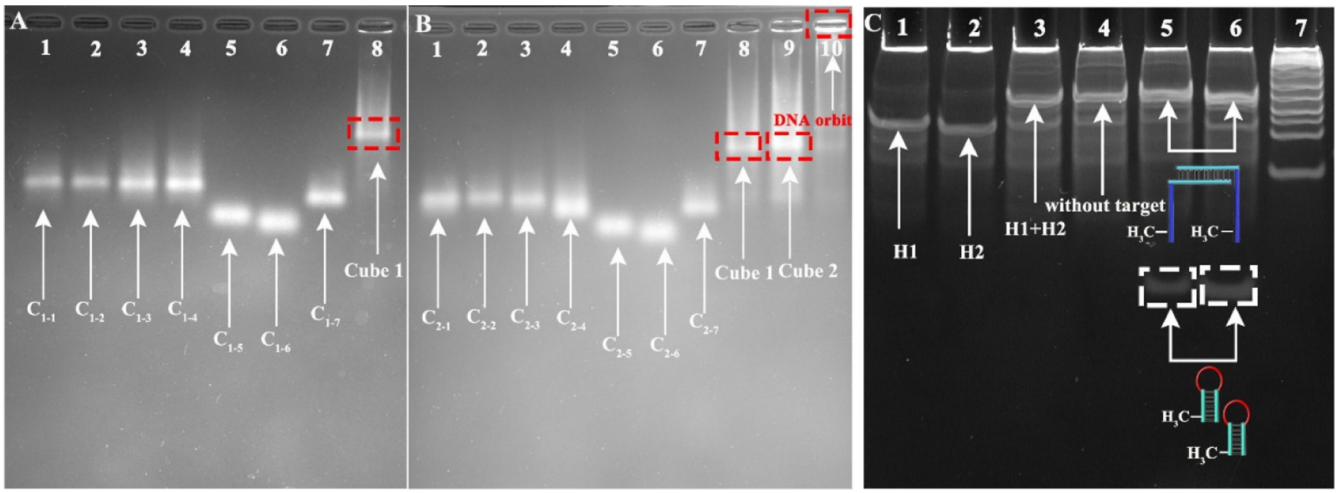

Figure 3. (A) AGE analysis of the DNA cube 1 self-assembly: lane 1: C_{1-1}; lane 2: C_{1-2}; lane 3: C_{1-3}; lane 4: C_{1-4}; lane 5: C_{1-5}; lane 6: C_{1-6}; lane 7: C_{1-7}; and lane 8: DNA cube 1. (B) AGE analysis of the DNA cube 2 and wireframe orbit self-assembly: lane 1: C_{2-1}; lane 2: C_{2-2}; lane 3: C_{2-3}; lane 4: C_{2-4}; lane 5: C_{2-5}; lane 6: C_{2-6}; lane 7: C_{2-7}; lane 8: cube 1; lane 9: cube 2; and lane 10: DNA wireframe. (C) Nondenaturing PAGE analysis of the bipedal DNA walker: lane 1: H1; lane 2: H2; lane 3: the mixture of H1 and H2 (DH); lane 4: the mixture of the DH, Dam, and Dpn1; lane 5: the mixture of DH, Dam, MTase, and Dpn1 (0.1 U); lane 6: the mixture of DH, Dam, MTase, and Dpn1 (10 U); lane 7: DNA marker (25, 50, 75, 100, 150, 200, 300, 400, and 500 bp).

ECL biosensor for Dam MTase activity detection based on the wireframe orbit-accelerated bipedal DNA walker. Benefiting from the methylated role of methyltransferase and cleavage action of endonuclease Dpn I in the same sequence of 5′-G-A-T-C-3′,[22,23] the bipedal walkers were converted from DH structures under the activation of the target. Meanwhile, the wireframe orbits decorated with ferrocene (Fc) as quenching probes on the top were modified on the Pd NPs/Rub@TiO_2/GCE to obtain the "signal off" state. When the bipedal walker autonomously and directionally moved on the DNA wireframe orbits, quenching molecules were released under the endonuclease role of Nt.BbvCI to restore the signal continuously ("signal on" state).

Scanning Electron Microscopy and Transmission Electron Microscopy Characterizations of the Prepared Materials. The morphologies and sizes of the prepared different materials were determined by employing scanning electron microscope (SEM) and transmission electron microscope (TEM). Compared with the SEM image of pure SiO_2 NPs with uniform diameters around 100 nm and smooth appearance (Figure 1A), the SEM image of TiO_2@SiO_2 NPs (Figure 1B) shows the monodispersed nanospheres with similar size and rough layer, identifying that SiO_2 NPs as rigid cores were coated by TiO_2. In the SEM image of Rub@TiO_2@SiO_2 NPs (Figure 1C), the much rougher and thicker layer of nanospheres verified the modification of Rub. From the TEM

https://doi.org/10.1021/acssensors.2c01262
ACS Sens. 2022, 7, 2475−2482

characterizations, the more exact morphologies of Rub@TiO_2@SiO_2 NPs before and after etching were presented. Before etching, Rub@TiO_2@SiO_2 NPs presented clear core−shell nanostructures, where TiO_2 and Rub almost completely coated the SiO_2 NPs (Figure 1D). After the etching of inner cores, there were hollow nanospheres with well-defined boundaries and interior cavities (Figure 1E), confirming the successful etching of SiO_2 sacrificial template. Furthermore, as clearly shown in the enlarged image of the Rub@TiO_2 NS surface (Figure 1F), the shell was composed of highly crystalline nanocrystals with the interplanar spacing of ∼0.239 nm corresponding to (004) planes of the anatase TiO_2 with excellent photoelectric activity.[24]

Optical Characterizations of the Prepared Hollow Material. The various optical characterizations of the prepared Rub@TiO_2 NSs were further investigated. As displayed in Figure 2A, the Rub@TiO_2 NSs displayed a fluorescent emission at 571.4 nm under the excitation wavelength of 500.6 nm. In addition, the UV−vis absorption spectra of rubrene with tetrahydrofuran (THF) as the solvent showed three bonds at 462, 491, and 526 nm, in line with the previous reports (Figure 2B), indicating the monodispersed state of Rub molecules.[12] However, the bathochromic shifts with varying degrees occurred in the UV−vis absorption spectra of the prepared Rub@TiO_2 NSs, where the absorption peaks appeared at 473, 512, and 564 nm, respectively. These results implied that the rubrene molecules as J-aggregates existed and larger conjugate systems were formed.[25] In addition, the ECL spectrum (Figure 2C) and 3D color map surface (Figure 2D) exhibit that the ECL emission wavelength of the Rub@TiO_2 NSs located at around 575 nm, which was similar with the fluorescent emission (571.4 nm), suggesting that the ECL of Rub@TiO_2 NSs was obtained by the intrinsic state formation of the Rub molecules rather than excimer formation.[26,27]

Gel Electrophoresis Characterizations of the DNA Wireframe and the Bipedal DNA Walker. Gel electrophoresis was used to verify the assemblies of DNA wireframe orbits and the bipedal DNA walker. First, 2% agarose gel electrophoresis (AGE) was used to characterize the assembly process of DNA wireframe orbits. As shown in Figure 3A, each one of the lanes from 1 to 7 showed a distinct band separately corresponding to C_{1-1} ∼ C_{1-7}, respectively. According to the principle that migration rate is inversely proportional to the base number of DNA, it was worth noting that lane 8 containing seven single-strand mixtures from C_{1-1} to C_{1-7} showed an obvious band with slower migration rate than any single strand, proving that seven single strands from C_{1-1} to C_{1-7} were successfully hybridized and assembled to form DNA cube 1. Similarly, lane 9 loading C_{2-1} ∼ C_{2-7} had the lowest migration rate compared to the seven lanes from C_{2-1} to C_{2-7} in Figure 3B, proving that cube 2 was also assembled successfully. Furthermore, compared to the individual DNA cubes (lanes 8 and 9), lane 10 containing the mixture of cubes 1 and 2 had a band on the top with the slowest migration rate, demonstrating the successful assembly of DNA wireframe orbits. Meanwhile, the assembly of bipedal DNA walkers was demonstrated by nondenaturing polyacrylamide gel electrophoresis (PAGE, 16%). As exhibited in Figure 3C, lanes 1 and 2 showed obvious bands and their migration rates were almost the same, which was consistent with the fact that the two lanes loaded single chains H1 and H2, respectively; while the band in lane 3 loading the mixture of H1 and H2 had a slower migration rate than that in lanes 1 and 2, which proved that the hybridization product (DH) of H1 and H2 appeared. As regards to lane 4 containing the complex of DH, SAM, and Dpn1, the bands displayed basically no change with lane 3, which proved that Dpn1 cannot play the endonuclease role in the absence of Dam MTase. While the lanes 5 and 6 containing all complexes of DH, SAM, Dam MTase, and Dpn 1, it was clearly observed that there were obvious bands at the bottom, which was attributed to the DNA rings cut from DH. Moreover, the bottom band in lane 6 was clearer than that in lane 5, proving that the higher the concentration of target Dam MTase was, the more DNA rings were cut and the more bipedal DNA walkers were generated for subsequent DNA amplification.

Atomic Force Microscopy Characterizations of the DNA Cube and DNA Wireframe Assembled by DNA Cubes. Atomic force microscopy (AFM) was further applied to characterize the individual DNA cubes and the DNA wireframe orbits assembled by DNA cubes. Figure 4A exhibits

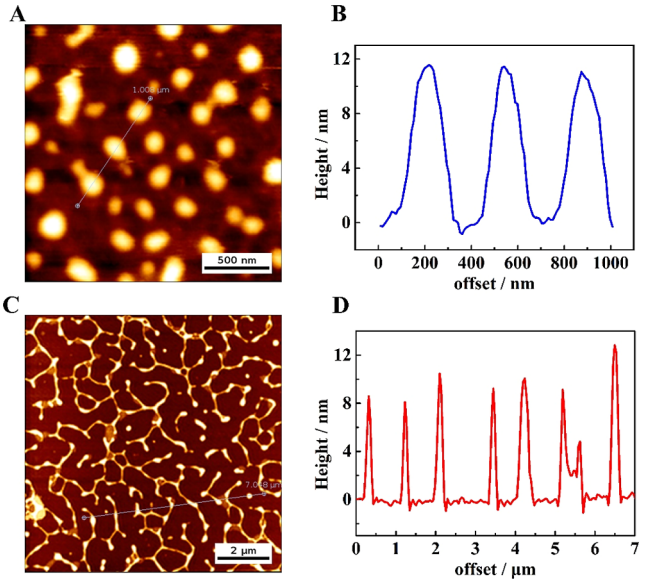

Figure 4. AFM images of DNA cubes (A) and DNA wireframe orbits (C). Height profile of the AFM images along the white line (B,D).

that many particles of comparable size were distributed at the interface, and the corresponding height profile (Figure 4B) shows the thickness of about ∼11 nm, which was close to the theoretical height of DNA cubes. The width was larger than the actual size due to the tip broadening effect, which would disrupt the judgment of the surface roughness and horizontal width.[28,29] This result demonstrated the successful formation of DNA cubes with uniform, scattered characteristics. As clearly depicted in the AFM image of DNA wireframe orbits (Figure 4C), there were paved network paths comprising many continuous lines with a length of micron scale, and compared with individual DNA cubes (Figure 4B), the DNA cube assembly led to no change in the height (Figure 4D), substantiating the formation of DNA wireframes by hybridization.

Comparison of the Walking Rate of Two Modes DNA Walkers Based on DNA Cubes and DNA Wireframe Orbits. To verify the promotion effect of DNA wireframe orbits, the walking kinetics of two modes DNA walkers were investigated by time-dependent ECL analysis for comparison.

https://doi.org/10.1021/acssensors.2c01262
ACS Sens. 2022, 7, 2475−2482

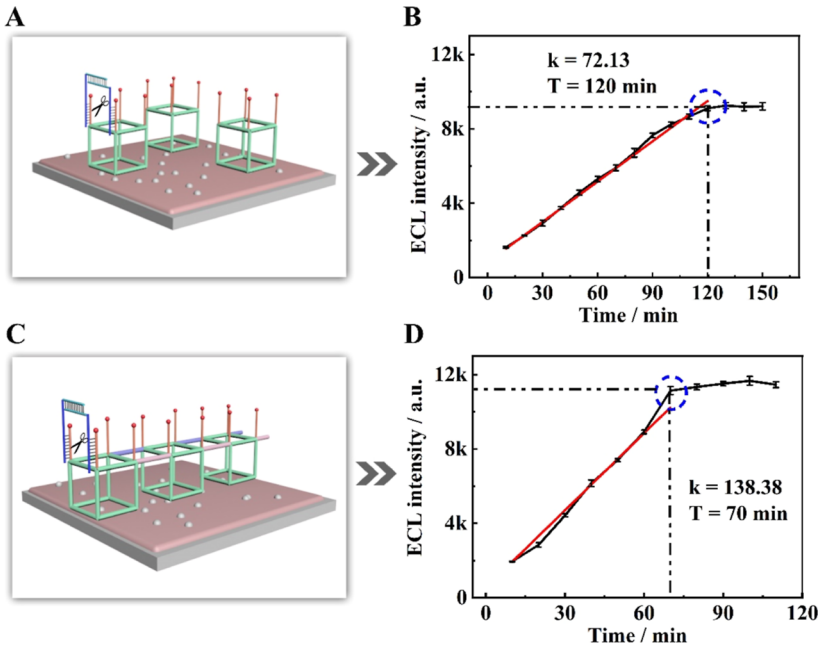

Figure 5. Working principle (A,C) and time-dependent ECL analysis (B,D) of the two modes DNA walkers based on DNA cubes and DNA wireframe orbits.

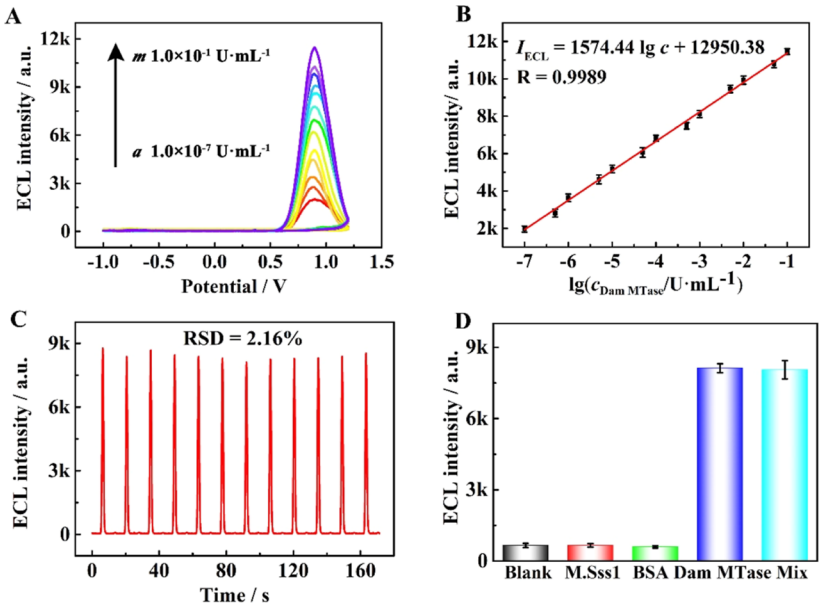

Figure 6. (A) ECL responses of the proposed biosensor to Dam MTase with different concentrations (Curves *a*−*m*: 1.0×10^{-7}, 5.0×10^{-7}, 1.0×10^{-6}, 5.0×10^{-6}, 1.0×10^{-5}, 5.0×10^{-5}, 1.0×10^{-4}, 5.0×10^{-4}, 1.0×10^{-3}, 5.0×10^{-3}, 1.0×10^{-2}, 5.0×10^{-2}, 1.0×10^{-1} U·mL^{-1}). (B) Calibration curve between the value of ECL signal intensities and the logarithm values of Dam MTase concentrations. (C) ECL stability and (D) specificity of the proposed biosensor.

When applying individual DNA cubes as the DNA orbits of the bipedal walkers (Figure 5A), the ECL intensity reached a plateau within 120 min and the walking rate (k) depending on the slope of ECL intensity−time curve was 72.13 (Figure 5B). Simultaneously, when applying the DNA wireframes rather than individual DNA cubes as DNA orbits (Figure 5C), the time to reach the platform was reduced to 70 min and the walking rate was increased to 138.38 markedly (Figure 5D). The nearly two-fold increase in walking rate indicated the improved kinetics using DNA wireframe as DNA orbits, further demonstrating that the wireframe orbit accelerated the moving of bipedal DNA walker.

Sensitivity, Stability, and Specificity of the Proposed Dam MTase Biosensor. To identify the detection sensitivity of the proposed biosensor, the quantitative activity detection of Dam MTase with different concentrations has been determined under the optimal conditions. Figure 6A illustrates that the ECL intensity increased gradually as the concentration of Dam MTase elevated from 1.0×10^{-7} to 1.0×10^{-1} U·mL^{-1} (curves *a*−*m*). Moreover, the ECL intensity presented a good linear correlation with the logarithm value of Dam MTase

https://doi.org/10.1021/acssensors.2c01262
ACS Sens. 2022, 7, 2475−2482

concentrations. In the calibration curve, the linear regression equation was $I = 1574.44 \log c + 12\,950.38$ (Figure 6B), where I was the ECL intensity and c was the Dam MTase concentration. Meanwhile, the limit of detection (LOD) was calculated to be 2.30×10^{-8} U·mL^{-1} using the 3σ method (S/N = 3).[30]

The stability and specificity as two principal elements were also explored to identify the detection capability of biosensor. After scanning 12 cycles continuously with the Dam MTase concentration of 5.0×10^{-4} U·mL^{-1}, the ECL responses almost remained stable with the relative standard deviation (RSD) of 2.16% (Figure 6C), demonstrating the acceptable stability of the proposed biosensor. To further verify the detection selectivity of the proposed biosensor for Dam MTase, the ECL responses were detected toward different proteins, including M.Sss1, BSA, Dam MTase, and their mixtures. As clearly depicted in Figure 6D, the ECL responses of BSA and M.Sss1 (10^{-1} U·mL^{-1}) were as weak as the background signal. It was apparent that the ECL signals containing the target Dam MTase were highest even if the concentration was down to 10^{-3} U·mL^{-1}, demonstrating the excellent specificity of the biosensor toward Dam MTase.

Feasibility of the Dam MTase Biosensor in Human Serum Sample. To investigate the feasibility of the Dam MTase biosensor in the real sample detection, the Dam MTase solutions were spiked with 50-fold diluted human serum to prepare real samples with different concentrations for the ECL test to evaluate the recovery of the biosensor. The found concentrations were calculated by the linear regression equation, and the recovery rates were calculated by the ratio of the found to added concentration. As shown in Table 1, the recovery rates were from 96.0 to 103%, and the RSD was from 1.1 to 2.0%. These results were within the acceptable range, substantiating the feasibility of the proposed biosensor in the actual sample for Dam MTase detection.

Table 1. Feasibility of the Dam MTase Biosensor in Human Serum Sample

sample	added (U·mL^{-1})	found (U·mL^{-1})	recovery (%)	RSD (%)
1	1.00×10^{-1}	9.60×10^{-2}	96.0	1.1
2	1.00×10^{-3}	1.03×10^{-3}	103	2.0
3	1.00×10^{-5}	9.92×10^{-6}	99.2	1.9

CONCLUSIONS

In summary, to cope with the challenges of traditional DNA walkers in walking dynamics and walking path controllability, the DNA wireframe orbit-accelerated bipedal DNA walker was designed skillfully here. The wireframe orbits assembled by DNA cubes have improved the efficiency and continuity of walking due to the enhancement of contact chance and the dynamic interaction between walking strands and designated orbits. Additionally, a ternary ECL system with the pore confinement-enhanced ECL performance was proposed, employing hollow Rub@TiO_2 as ECL emitters, endogenous dissolved oxygen as the coreactant, and Pd NPs as coreaction accelerators. Eventually, the bipedal walkers activated by the target can directionally walk on the DNA wireframe orbits to release the quenching probes continuously for the sensitive detection of Dam MTase activity applying the Rub-based ECL system. Therefore, the construction process of biosensor for Dam MTase activity is expected to be applied to other MTase detection techniques in biomedical studies and the clinical evaluation of drug efficacy.

ASSOCIATED CONTENT

Supporting Information

The Supporting Information is available free of charge at https://pubs.acs.org/doi/10.1021/acssensors.2c01262.

Reagents and materials and apparatus used in this work, preparation of palladium nanoparticles, morphology characterizations of palladium nanoparticles, optimization of experimental conditions, ECL and CV characterizations of the biosensor establishment process, and inhibitor of Dam MTase (PDF)

AUTHOR INFORMATION

Corresponding Author

Ying Zhuo − *Key Laboratory of Luminescence Analysis and Molecular Sensing (Southwest University), Ministry of Education, College of Chemistry and Chemical Engineering, Southwest University, Chongqing 400715, PR China;* orcid.org/0000-0002-4491-1186; Phone: +86 23 68253172; Email: yingzhuo@swu.edu.cn; Fax: +86 23 68253172

Authors

Mei-Chen Pan − *Key Laboratory of Luminescence Analysis and Molecular Sensing (Southwest University), Ministry of Education, College of Chemistry and Chemical Engineering, Southwest University, Chongqing 400715, PR China*

Mao-Hua Gao − *Key Laboratory of Luminescence Analysis and Molecular Sensing (Southwest University), Ministry of Education, College of Chemistry and Chemical Engineering, Southwest University, Chongqing 400715, PR China*

Xia Yang − *Key Laboratory of Luminescence Analysis and Molecular Sensing (Southwest University), Ministry of Education, College of Chemistry and Chemical Engineering, Southwest University, Chongqing 400715, PR China;* orcid.org/0000-0003-0897-2106

Wen-Bin Liang − *Key Laboratory of Luminescence Analysis and Molecular Sensing (Southwest University), Ministry of Education, College of Chemistry and Chemical Engineering, Southwest University, Chongqing 400715, PR China;* orcid.org/0000-0002-9086-4974

Ruo Yuan − *Key Laboratory of Luminescence Analysis and Molecular Sensing (Southwest University), Ministry of Education, College of Chemistry and Chemical Engineering, Southwest University, Chongqing 400715, PR China;* orcid.org/0000-0003-3664-6236

Complete contact information is available at: https://pubs.acs.org/10.1021/acssensors.2c01262

Notes

The authors declare no competing financial interest.

ACKNOWLEDGMENTS

This work was financially supported by the NNSF of China (22022408), the Chongqing Talents·Youth Top-notch Personnel Support Program (CQYC201905067), and the Fundamental Research Funds for the Central Universities (XDJK2019TJ002), China.

REFERENCES

(1) Jung, C.; Allen, P. B.; Ellington, A. D. A simple, cleated DNA walker that hangs on to surfaces. *ACS Nano* **2017**, *11*, 8047−8054.

(2) Li, N.; Du, M.; Liu, Y.; Ji, X.; He, Z. Multipedal DNA walker biosensors based on catalyzed hairpin assembly and isothermal strand-displacement polymerase reaction for the chemiluminescent detection of proteins. *ACS Sens.* **2018**, *3*, 1283−1290.

(3) Liu, M.; Cheng, J.; Tee, S. R.; Sreelatha, S.; Loh, I. Y.; Wang, Z. Biomimetic autonomous enzymatic nanowalker of high fuel efficiency. *ACS Nano* **2016**, *10*, 5882−5890.

(4) Liber, M.; Tomov, T. E.; Tsukanov, R.; Berger, Y.; Nir, E. A bipedal DNA motor that travels back and forth between two DNA origami tiles. *Small* **2015**, *11*, 568−575.

(5) Ge, Z.; Gu, H.; Li, Q.; Fan, C. Concept and development of framework nucleic acids. *J. Am. Chem. Soc.* **2018**, *140*, 17808−17819.

(6) Yang, F.; Yao, J. S.; Bu, S. C.; Meng, H. Y.; Zhuo, Y.; Zhong, X.; Yuan, R. Quadrilateral nucleic acid frame-accelerating DNAzyme walker kinetics for biosensing based on host-guest recognition-enhanced electrochemiluminescence. *Anal. Chem.* **2021**, *93*, 15493−15500.

(7) Bujold, K. E.; Hsu, J. C. C.; Sleiman, H. F. Optimized DNA "Nanosuitcases" for encapsulation and conditional release of siRNA. *J. Am. Chem. Soc.* **2016**, *138*, 14030−14038.

(8) Liao, N.; Pan, M. C.; Wang, L.; Yang, F.; Yuan, R.; Zhuo, Y. Swing arm location-controllable DNA walker for electrochemiluminescence biosensing. *Anal. Chem.* **2021**, *93*, 4051−4058.

(9) Ostroverkhova, O. Organic optoelectronic materials: mechanisms and applications. *Chem. Rev.* **2016**, *116*, 13279−13412.

(10) Bezman, R.; Faulkner, L. R. Mechanisms of chemiluminescent electron-transfer reactions. V. Absolute measurements of rubrene luminescence in benzonitrile and *N,N*-dimethylformamide. *J. Am. Chem. Soc.* **1972**, *94*, 6324−6330.

(11) Najafov, H.; Lyu, B.; Biaggio, I.; Podzorov, V. Two mechanisms of exciton dissociation in rubrene single crystals. *Appl. Phys. Lett.* **2010**, *96*, 183302.

(12) Yang, S. S.; Jiang, M. H.; Chai, Y. Q.; Yuan, R.; Zhuo, Y. Application of antibody-powered triplex-DNA nanomachine to electrochemiluminescence biosensor for the detection of anti-digoxigenin with improved sensitivity versus cycling strand displacement reaction. *ACS Appl. Mater. Interfaces* **2018**, *10*, 38648−38655.

(13) Wang, M.; Hu, Y.; Han, J.; Guo, R.; Xiong, H.; Yin, Y. TiO_2/NiO hybrid shells: p-n junction photocatalysts with enhanced activity under visible light. *J. Mater. Chem. A* **2015**, *3*, 20727−20735.

(14) Li, W.; Wu, Z.; Wang, J.; Elzatahry, A. A.; Zhao, D. A Perspective on Mesoporous TiO_2 Materials. *Chem. Mater.* **2013**, *26*, 287−298.

(15) Wang, Q.; Pan, M.; Wei, J.; Liu, X.; Wang, F. Evaluation of DNA methyltransferase activity and inhibition via isothermal enzyme-free concatenated hybridization chain reaction. *ACS Sens.* **2017**, *2*, 932−939.

(16) Li, C.; Wang, H.; Shang, J.; Liu, X.; Yuan, B.; Wang, F. Highly Sensitive Assay of Methyltransferase Activity Based on an Autonomous Concatenated DNA Circuit. *ACS Sens.* **2018**, *3*, 2359−2366.

(17) Zhong, X.; Yang, S. S.; Liao, N.; Yuan, R.; Zhuo, Y. Development of hollow electrochemiluminescent nanocubes combined with a multisite-anchored DNA nanomachine for mycotoxin detection. *Anal. Chem.* **2021**, *93*, 5301−5308.

(18) Zhou, Y. C.; Ran, X. X.; Chen, A. Y.; Chai, Y. Q.; Yuan, R.; Zhuo, Y. Efficient electrochemical self-catalytic platform based on L-Cys-hemin/G-quadruplex and its application for bioassay. *Anal. Chem.* **2018**, *90*, 9109−9116.

(19) Wang, X.; Bai, L.; Liu, H.; Yu, X.; Yin, Y.; Gao, C. A unique disintegration−reassembly route to mesoporous titania nanocrystalline hollow spheres with enhanced photocatalytic activity. *Adv. Funct. Mater.* **2017**, *28*, 1704208.

(20) Xiang, Y.; Li, Y.; Zhang, X.; Zhou, A.; Jing, N.; Xu, Q. Hybrid Cu_xO-TiO_2 porous hollow nanospheres: preparation, characterization and photocatalytic properties. *RSC Adv.* **2017**, *7*, 31619−31627.

(21) Chen, A. Y.; Ma, S. Y.; Zhuo, Y.; Chai, Y. Q.; Yuan, R. In situ electrochemical generation of electrochemiluminescent silver nanoclusters on target-cycling synchronized rolling circle amplification platform for microRNA detection. *Anal. Chem.* **2016**, *88*, 3203−3210.

(22) Li, J.; Yan, H.; Wang, K.; Tan, W.; Zhou, X. Hairpin fluorescence DNA probe for real-time monitoring of DNA methylation. *Anal. Chem.* **2007**, *79*, 1050−1056.

(23) Wu, J.; Hu, Q.; Chen, Q.; Dai, J.; Wu, X.; Wang, S.; Lou, X.; Xia, F. Modular DNA-incorporated aggregation-induced emission probe for sensitive detection and imaging of DNA methyltransferase. *ACS Appl. Bio Mater.* **2020**, *3*, 9002−9011.

(24) Qu, X.; Liu, M.; Li, L.; Wang, C.; Zeng, C.; Liu, J.; Shi, L.; Du, F. Fabrication of CdTe QDs/BiOI-promoted TiO_2 hollow microspheres with superior photocatalytic performance under simulated sunlight. *Nanoscale Res. Lett.* **2019**, *14*, 50.

(25) Mahajan, P. G.; Bhopate, D. P.; Kamble, A. A.; Dalavi, D. K.; Kolekar, G. B.; Patil, S. R. Selective sensing of Fe^{2+} ions in aqueous solution based on fluorescence quenching of SDS capped rubrene nanoparticles: application in pharmaceutical formulation. *Anal. Methods* **2015**, *7*, 7889−7898.

(26) Wu, P.; Hou, X.; Xu, J. J.; Chen, H. Y. Electrochemically generated versus photoexcited luminescence from semiconductor nanomaterials: bridging the valley between two worlds. *Chem. Rev.* **2014**, *114*, 11027−11059.

(27) Suk, J.; Wu, Z.; Wang, L.; Bard, A. J. Electrochemistry, electrogenerated chemiluminescence, and excimer formation dynamics of intramolecular π-stacked 9-naphthylanthracene derivatives and organic nanoparticles. *J. Am. Chem. Soc.* **2011**, *133*, 14675−14685.

(28) Lyubchenko, Y. L.; Shlyakhtenko, L. S. AFM for analysis of structure and dynamics of DNA and protein-DNA complexes. *Methods* **2009**, *47*, 206−213.

(29) Kvien, I.; Tanem, B. S.; Oksman, K. Characterization of cellulose whiskers and their nanocomposites by atomic force and electron microscopy. *Biomacromolecules* **2005**, *6*, 3160−3165.

(30) Long, G. L.; Winefordner, J. D. Limit of detection. A closer look at the IUPAC definition. *Anal. Chem.* **1983**, *55*, 712A−724A.

https://doi.org/10.1021/acssensors.2c01262
ACS Sens. 2022, 7, 2475−2482